RADIAL TEMPERATURE DISTRIBUTIONS OF C^{6+} IONS IN THE TEXTOR EDGE PLASMA MEASURED WITH LITHIUM BEAM ACTIVATED CHARGE EXCHANGE SPECTROSCOPY

R.P. SCHORN, E. WOLFRUM*, F. AUMAYR*,
E. HINTZ, D. RUSBÜLDT, H. WINTER*
Institut für Plasmaphysik,
Forschungszentrum Jülich GmbH,
Association Euratom-KFA,
Jülich, Germany

ABSTRACT. A new method of obtaining the temperature of highly charged carbon ions in the boundary layer of tokamak discharges is described. Lithium beam activated charge exchange spectroscopy (Li-CXS) has been employed to measure the spectral profiles of the optical radiation following the electron transfer between impurity ions and a neutral lithium diagnostic beam. By assuming a Maxwellian velocity distribution, ion temperatures are deduced fitting a Gaussian profile to Doppler broadened charge exchange emission lines. Additional line broadening caused by magnetic fields (Zeeman effect) and collisional ℓ-level mixing of the upper electronic state, which may both give rise to several overlapping transitions of slightly different wavelengths, is discussed. The method does not depend on the presence of neutral injection heating beams and is therefore useful for investigating various heating situations, such as Ohmic discharges, beam heated plasmas and high frequency heated plasmas, as well as combinations thereof. The paper presents measurements of ohmically heated and beam heated discharges and discusses their implications with regard to the determination of the plasma D^+ temperature and the amount of carbon removed from limiter surfaces owing to $C^{6+} \rightarrow C$ self-sputtering.

1. INTRODUCTION

Injection of a beam of fast neutral lithium atoms into a tokamak boundary plasma provides a wide range of diagnostic possibilities [1]. Important plasma parameters, such as electron densities, electric and magnetic fields, and densities and temperatures of highly charged impurity ions, can be measured by analysing the optical radiation following collisions of lithium atoms with plasma particles. Lithium beam activated charge exchange spectroscopy (Li-CXS), for example, gives access to the highly ionized states of one of the dominant impurity species in present day tokamak devices, namely carbon [2]. In this paper we describe the application of Li-CXS to the measurement of radial temperature profiles of the fully stripped C^{6+} in the boundary layer of the TEXTOR tokamak by analysing the spectral line shape of the charge exchange induced radiation and we discuss the feasibility of deriving the plasma ion temperature kT_{D+} from the data obtained for C^{6+}. First results are shown for ohmically and beam heated shots which, together with the absolute C^{6+} densities published in Ref. [2], allow to estimate the amount of carbon eroded from the limiter surfaces owing to physical $C^{6+} \rightarrow C$ self-sputtering.

2. METHOD

The method employed is based on the fact that a C^{6+} impurity ion may capture the weakly bound outer electron of an injected fast lithium atom, which should preferably have energies between 20 and 30 keV. Considering the most probable couplings in the collisional quasi-molecule $[C\text{-}Li]^{6+}$ during the charge exchange process, it is concluded that this electron will preferentially move into highly excited states of $C^{5+}(n, \ell)$. Consequently, characteristic line radiation of this carbon ion will be emitted:

$$C^{6+} + Li^0 \rightarrow (C^{5+} + h\nu) + Li^+ \qquad (1)$$

As recently observed spectroscopically [3], this charge exchange process specifically leads to hydrogenic C^{5+}

* *Permanent address:* Institut für Allgemeine Physik, Technische Universität Wien, Wiedner Hauptstraße 8-10, A-1040 Vienna, Austria.

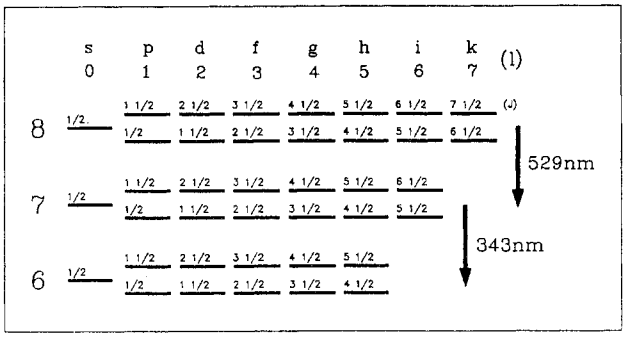

FIG. 1. Part of the electronic energy level diagram of C^{5+} relevant to the charge exchange process studied. After charge exchange, electrons are captured mainly into the 7th and 8th principal shells with high ℓ-values, giving rise to optical radiation at 343 nm and 529 nm. Owing to ℓ-level mixing (see Section 4), all allowed dipole transitions can be observed simultaneously.

ions with their outer electrons in ($n = 7$, $\ell = 4...6$) and ($n = 8$, $\ell = 5...7$) states (see Fig. 1). Thus, a rapid radiative decay process can be observed, for example at wavelengths of 343 nm and 529 nm. The radiation intensity I_λ can be estimated in terms of photons/cm^3·s from the following expression:

$$I_\lambda = N_{C6+}\Phi_{Li}\sigma_\lambda \qquad (2)$$

where N_{C6+} is the absolute density of the fully stripped carbon nuclei, Φ_{Li} is the flux density of the fast lithium probing beam and σ_λ is the charge exchange emission cross-section at the respective wavelength. The latter quantity has recently been determined experimentally [3]. For a monoenergetic beam of 20 keV, for example, values of 3.5×10^{-15} cm^2 (529 nm) and 1.2×10^{-14} cm^2 (343 nm) have been found; these values are about two orders of magnitude higher than the corresponding values for neutral hydrogen beams [4, 5]. The current densities of the fast Li^0 probing beams necessary to ensure a C^{6+} detection limit of less than 10^{10} cm^{-3} may therefore be relatively low (a few mA/cm^2). All kinds of plasma heating can thus be studied with Li-CXS, including pure Ohmic shots and radiofrequency (RF) heated shots, without the necessity of employing a H/D heating beam, which itself would strongly influence the properties of the plasma. Although the line at 529 nm has a lower production cross-section because the electron transfer predominantly leads to ($n = 7$) states, we concentrate in our discussion on the transition corresponding to this line because of experimental convenience (glass optics and visible light throughout) and because the signal intensities are high enough, since the detection limit is not defined by the properties of the detector but by the ratio of the beam produced charge exchange intensity and the radiation originating from the same transition, which is caused by charge exchange of C^{6+} with cold neutral hydrogen at the boundary and by collisional excitation of C^{5+}. This ratio is not expected to differ significantly at 343 nm and 529 nm. A more detailed outline of Li-CXS, taking into account modelling of the beam–plasma interaction and the determination of absolute ion densities, is given in Ref. [2]. We concentrate here mainly on the measurement of ion impurity temperatures. For this purpose, we use the Doppler broadening of the charge exchange radiation emitted according to Eq. (1) and analyse its spectral profile. Under the assumption of a thermal Maxwellian velocity distribution for C^{6+}, the spectral line shape of a single transition is expressed by the Gaussian profile

$$S(\lambda) \propto \exp\left[-\left(\frac{\lambda - \lambda_0}{\Delta\lambda}\right)^2\right] \qquad (3)$$

where λ_0 is the central wavelength of this profile and $\Delta\lambda$ characterizes the profile width. The ion temperature kT_{C6+} is obtained from a least squares fit of $\Delta\lambda$, λ_0 and a scale factor to Eq. (3) in the usual way by applying the relation

$$\Delta\lambda = \frac{\lambda_0}{c}\sqrt{\frac{2kT_{C6+}}{m}} \qquad (4)$$

where m is the mass of the carbon atom (1.99×10^{-26} kg) and c is the velocity of light.

3. CONSIDERATION OF ZEEMAN BROADENING

Two processes can alter the spectral line shape of the charge exchange produced light independently of kT_{C6+} and, therefore, special consideration of these processes is needed. In tokamak edge plasmas, we usually find magnetic fields of more than 2 T. Consequently, the Zeeman splitting of electronic energy levels and an apparent non-thermal line broadening caused by this effect should be examined. The Zeeman shift $\Delta\lambda_Z$ of a transition wavelength λ is expressed [6] by

$$\Delta\lambda_Z = \frac{\lambda^2}{hc}\mu_B B(M_2 g_2 - M_1 g_1) \qquad (5)$$

TABLE I. LANDÉ FACTORS FOR THE $(n = 8, \ell = 7) \rightarrow (n = 7, \ell = 6)$ TRANSITION OF THE C^{5+} ION

n = 8	J = 7½	$g_2 = 1.067$
	J = 6½	$g_2 = 0.933$
n = 7	J = 6½	$g_1 = 1.077$
	J = 5½	$g_1 = 0.923$

where μ_B is the Bohr magneton (9.274×10^{-24} J/T), B is the magnetic field, $M_{1,2}$ are the magnetic quantum numbers of the upper and lower levels ($M_{1,2} = -\ell_{1,2} \ldots +\ell_{1,2}$), and $g_{1,2}$ are Landé factors of the corresponding multiplets. In Ref. [7], theoretical g-factors have been tabulated for doublet configurations, such as those of C^{5+}. Table I presents values of the $(n = 8, \ell = 7) \rightarrow (n = 7, \ell = 6)$ transition at 529.1 nm, which is the most intense transition for these two shells. From Eq. (5) and Table I, the mean total splitting of the Zeeman lines ($2\Delta\lambda_Z$) can be calculated.

For the π-component ($\Delta M = 0$), the spacing is negligibly small. The σ-components ($\Delta M = \pm 1$) can, however, show considerable splittings. In cases where the line intensity cannot be corrected through suppression of the unfavourable σ-component by a linear polarizer, or where observation is only possible in parallel to the magnetic field, the effect of Zeeman splitting on the spectral shape of the charge exchange line has to be studied in detail. If, however, the line splittings are small with respect to the Doppler width of the transition, as is the case for temperatures above 30 eV and magnetic fields below 3 T, we can simplify these studies by treating the total profile of all Zeeman lines present as a single, but broadened, 'quasi-Gaussian'. With the help of intensity rules for the Zeeman effect [8], we have computed the additional broadening with respect to pure thermal Doppler widths for typical ion temperatures and magnetic fields as expected in tokamak boundary regions. Thus, a derating factor η_{Zeeman} can be derived for the raw kT_{C6+} values by taking the square of FWHM ratios of single and multiple profiles. If no account were taken of the Zeeman broadening, the temperatures determined would be systematically too high. Figure 2 shows correction factors calculated in this way for the most intense transition between n = 8 and n = 7 (i.e. $J = 7\frac{1}{2} \rightarrow J = 6\frac{1}{2}$) and magnetic fields of 1, 2 and 3 T. Here, simultaneous recording of the σ-component and the π-component perpendicular to $\vec{B}$ has been assumed. Use of σ-radiation only, for example when observation is only possible parallel to $\vec{B}$, leads to even smaller derating factors.

The absolute value of the total magnetic field should be known to an error of $\pm 10\%$ if an accuracy of better than 5% is required for the calculation of the derating factor at ion temperatures between 50 and 250 eV and magnetic fields below 3 T (see Fig. 2). At higher temperatures, the value of B_{total} influences the value of η_{Zeeman} by at most 10%. In TEXTOR, the deviation of the orientation of the magnetic field from the horizontal plane amounts to a maximum of 5–7°. If the observation geometry is chosen perpendicular to the equator, the derating factors will not be much lowered because of relative growth of σ-radiation.

For convenience in computation, the derating factors η_{Zeeman} of Fig. 2 have been fitted by the analytical function

$$\eta_{Zeeman} = a\,[\ln(kT_{C6+} - d)]^2 + b\,\ln(kT_{C6+} - d) + c \qquad (6)$$

where a, b, c and d represent the sets of fitting parameters, given in Table II, assuming kT_{C6+} in eV.

In the boundary region of TEXTOR plasmas, ion temperatures of 30–300 eV are expected for ohmically heated discharges, while values of up to 500 eV and even more may be reached during additional heating.

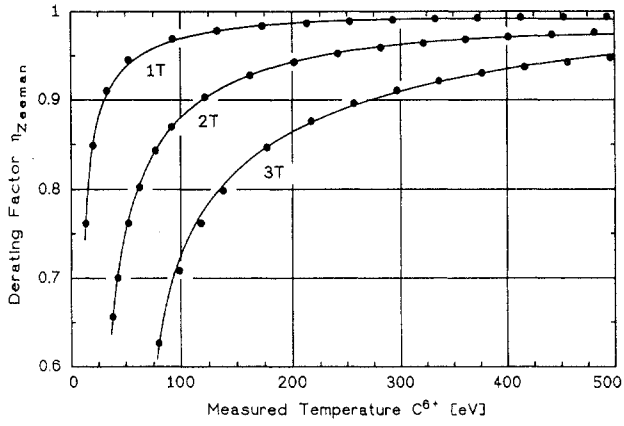

FIG. 2. Corrective derating factors η_{Zeeman} calculated taking into account Zeeman splitting for temperatures of C^{6+} measured by Doppler broadening of optical charge exchange radiation. Values for the strongest transition between the 8th shell and the 7th shell of C^{5+}, i.e. $J = 7\frac{1}{2} \rightarrow J = 6\frac{1}{2}$ at 529.1 nm, are shown for magnetic fields of 1, 2 and 3 T. Simultaneous observation of the σ- and π-components perpendicular to $\vec{B}$ has been assumed. The solid lines represent analytical fits according to Eq. (6) and Table II. The temperature axis shows non-corrected values obtained from the raw data by a least squares fit to a single Gaussian profile.

TABLE II. FITTING PARAMETERS FOR η_{Zeeman} USING Eq. (6)

	1 T	2 T	3 T
a	-0.01145	-0.02346	-0.01362
b	+0.1354	+0.2977	+0.2258
c	+0.5916	+0.03054	+0.08185
d	+8.954	+23.86	+61.43

From the analysis shown in Fig. 2, we realize that the Zeeman effect cannot be neglected in this temperature range. Magnetic fields of, for example, 2 T lead to temperature errors of +3% to +25%, depending on the value of kT_{C6+}. For C^{6+} temperatures below about 500 eV, the values obtained by a single Gaussian fit have to be corrected using Eq. (6) if σ-radiation cannot be suppressed in the experiment by utilizing suitable polarization filters.

4. CONSIDERATION OF ℓ-LEVEL MIXING

There is another process which may also give rise to non-thermal broadening of charge exchange lines. Under certain conditions, C^{5+} particles resulting from charge exchange of neutral lithium with C^{6+} may collide with other plasma ions (predominantly D^+) and cause transfer between the different electronic ℓ-states of the same principal n-shell before the charge exchange electrons drop to a lower level under photon emission. Depending on the specific plasma conditions, the inverse ion-ion collision frequency can be much smaller than the lifetime of a level with respect to radiative decay. This phenomenon, called 'collisional ℓ-level mixing', is discussed in Ref. [9] for tokamak plasmas, with emphasis on the application of charge exchange spectroscopy using hydrogen heating beams. From Ref. [9], an empirical expression for hydrogenic ions can be derived which gives the critical effective quantum number n_{mix} indicating the lowest quantum level to be completely ℓ-mixed, corresponding to a statistical population of all (ℓ, m) sublevels:

$$n_{mix} \geq -2.14 + 1.71 \log_{10}\left(\frac{q^6 \sqrt{kT_i}}{Z_{eff} N_e}\right) \qquad (7)$$

Here, q is the ion charge, kT_i is the ion temperature in keV, N_e is the electron density of the plasma in units of 10^{13} cm^{-3} and Z_{eff} is the effective ion charge. An analysis of Eq. (7) for typical tokamak boundary plasmas (q = 5, N_e between 1×10^{12} and 3×10^{13} cm^{-3}, kT_i between 30 and 500 eV) shows that C^{5+} can be regarded as being completely mixed above the n = 4 shell, assuming that Z_{eff} is between 1.5 and 2. Equation (7) is a linear approximation of a more complicated relation and will be valid for $n_{mix} < 11$. 'Complete mixing' means that the population of all ℓ-levels is proportional to their statistical weights $(2\ell + 1)/n^2$ at any time, regardless of the process by which the electrons reached the specific principal shell and the ℓ-state into which they entered. Therefore, cascade processes originating from higher shells can be disregarded. Collisional ℓ-mixing implies not only that a single emission line will occur after charge transfer but also that the whole set of allowed transitions between, for example, the 8th and 7th shell will be observed simultaneously (see Figs 1 and 3). These lines have to be superimposed on each other to form a sum profile by using their correct central wavelengths and relative intensities. Since the wavelengths differ only very slightly, the various lines cannot be resolved, and the result may be treated in a similar way as the Zeeman line splitting in Section 3, as a single, broadened 'quasi-Gaussian' $I_{mix}(\lambda)$, represented by

$$I_{mix}(\lambda) \propto \sum_{8 \to 7} (2\ell + 1)\, \chi\, A_{\ell,\ell\pm1}\, S_{\ell,\ell\pm1}(\lambda) \qquad (8)$$

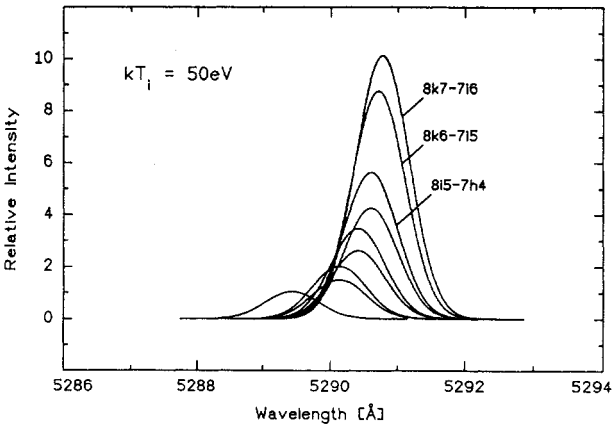

FIG. 3. Spectral profiles of the most intense transitions between the 8th and the 7th principal shells of C^{5+}, calculated for an ion temperature of 50 eV on the assumption of pure thermal Doppler broadening.

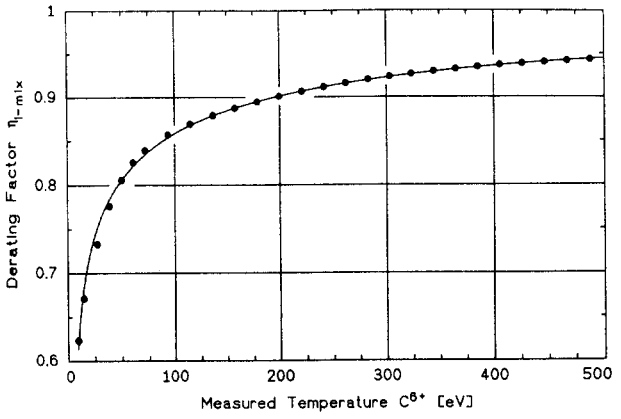

FIG. 4. Corrective derating factors $\eta_{\ell\text{-mix}}$ due to a complete statistical ℓ-mixing for temperatures of C^{6+} measured by Doppler broadening of optical charge exchange radiation. The solid line is an analytical fit according to Eq. (6) and the fitting parameters a–d listed above. The temperature axis gives non-corrected values obtained from the raw data by a least squares fit to a single Gaussian profile.

The sum has to be taken over all 37 allowed electric dipole transitions between n = 8 and n = 7, according to the selection rules $\Delta\ell = \pm 1$ and $\Delta J = 0, \pm 1$. $S_{\ell,\ell\pm1}(\lambda)$ is a single, purely Doppler broadened Gaussian line represented by Eq. (3), where the central wavelengths λ_0 have been derived from atomic energy levels of C^{5+} found in Ref. [10]. The Einstein coefficients of spontaneous emission, $A_{\ell,\ell\pm1}$, have been obtained from Refs [11, 12], while the intensity ratios χ of the fine-structure lines within a given $\ell \rightarrow \ell \pm 1$ transition have been calculated according to Ref. [13]. Figure 3 shows the most intense spectral profiles of the n = 8 → n = 7 transition calculated in this way, assuming an ion temperature of 50 eV. The transitions dominating the sum profile are those showing maximum ℓ- and J-numbers, e.g. 8k7 → 7i6 or 8k6 → 7i5. The central wavelengths involved vary over a range of 0.15 nm, justifying the treatment of the sum as a single additionally broadened line.

On the basis of previous considerations by Fonck et al. [9], a derating factor $\eta_{\ell\text{-mix}}$ due to ℓ-mixing can now be computed in the same way as for the Zeeman effect. The corresponding values are plotted in Fig. 4, where it can be seen that the temperature error ranges from +5% to +20% if ℓ-level mixing is neglected for typical edge plasma parameters. For convenience, the derating values $\eta_{\ell\text{-mix}}$ of Fig. 4 have also been fitted to the analytical function (6), again delivering the fitting parameters a, b, c and d (kT_{C6+} is in eV):

a	-0.008273
b	+0.1422
c	+0.3809
d	+2.868

5. EXPERIMENTAL

A high current fast lithium beam injector has been installed at TEXTOR (see Fig. 5). The device is based on a metal vapour ion source and can produce a Li^+ beam of 20–30 keV energy and a total current of up to 80 mA at the acceleration grids. At the plasma boundary in TEXTOR, the beam diameter is 40 mm; the equivalent total current after mass analysing in a focusing magnetic field configuration and neutralizing in a thermal lithium vapour cell is 5–10 mA. The resulting Li^0 beam hits the plasma edge radially with respect to the torus in the equatorial midplane. To discriminate between Li-CXS photons and radiation originating from the same C^{5+} transition, but produced by charge exchange with neutral atomic hydrogen in the scrape-off layer and by collisions of C^{5+} with plasma particles, the arc voltage of the discharge chamber of the ion source is pulsed with a frequency of 250 Hz. Consequently, a chopped Li^0 beam superimposes a charge exchange modulation upon the more or less continuous background radiation. In TEXTOR the beam has a mean penetration depth of typically 25 cm into ohmically heated plasmas and roughly 15 cm into additionally heated discharges, depending on the plasma parameters.

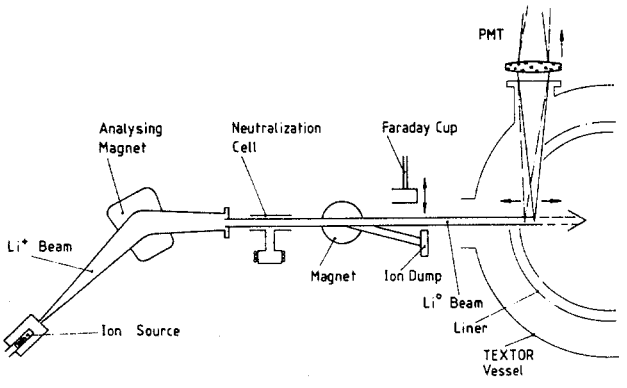

FIG. 5. Set-up of the Li-CXS experiment at TEXTOR: Generation and injection of the neutral lithium probing beam. A detailed description is given in Ref. [14].

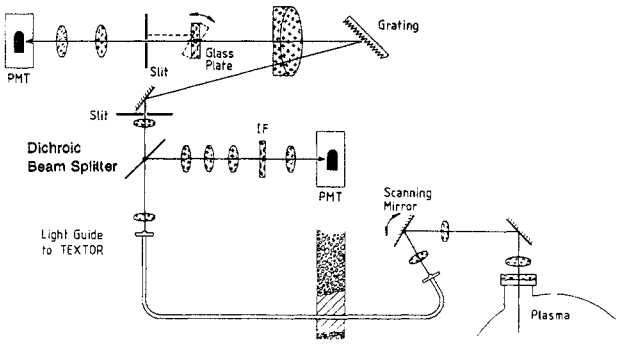

FIG. 6. Set-up of the Li-CXS experiment at TEXTOR: Detection of the optical radiation due to the interaction of the neutral lithium probing beam with the edge plasma. Spectrometer: 1200 lines/mm; blazed at 1400 nm, aperture 1:5.5; apparatus width 42 pm at 529 nm; accessible: 380–800 nm; scanning frequency 4 Hz.

A more detailed description of the properties of the injector and the technical features is given in Ref. [14].

The optical charge exchange radiation is detected spectrally and spatially and/or is resolved in time by means of a photomultiplier tube (PMT) and a large aperture (1:5.5) spectrometer with a focal length of 800 mm, situated outside the TEXTOR bunker and coupled to the plasma by means of a low-loss quartz fibre optical light guide of 10 m length (see Fig. 6). The spectrometer is fitted with a grating of 1200 lines/mm, in first order blazed at 1400 nm. A spectral scan is obtained by shifting the spectrum across the exit slit of the instrument by means of an electrically driven scanner consisting of a rectangular, 30 mm thick, glass block which can be tilted by maximally $\pm 15°$. During the experiments described below, the entrance slit was adjusted to a size of 0.1×10 mm. The measured apparatus width of the device was 0.042 nm at a wavelength of 529 nm, allowing the ion temperatures to be determined to values as low as about 30 eV. A complete spectral scan can be made within 125 ms (scanning frequency 4 Hz). Close to the entrance slit of the spectrometer, a dichroic beam splitter separates the wavelengths below and above 600 nm. An appropriate interference filter with a central wavelength of 670.8 nm permits observation of the basic Li^0 resonance line and thus determination of the beam attenuation [2]. The absolute signal intensity of the charge exchange line at 529 nm is not lowered by this measure. To improve the signal to noise ratio, several spectra are averaged over the stationary phases of TEXTOR discharges, the detection line being at a fixed radial position, which is altered stepwise from shot to shot. Radial scans may, however, be obtained by means of an electrically driven tilting mirror with frequencies of up to 4 Hz. The various raw data signals [2] are digitized by an eight channel ADC, employing a sampling rate of 10 kHz and a resolution of 12 bit. The experimental data are stored on a VAX 8800 computer for further digital after-shot processing.

6. RESULTS

To demonstrate the capabilities of Li-CXS, we show in Figs 7 and 8 radial profiles of the C^{6+} ion temperature as measured by the method outlined in the previous sections, for different plasma regimes. Each profile was obtained in a series of reproducible TEXTOR discharges because, at present, only a single radial location is recorded during one shot (see Section 5). Common features of all the discharges under investigation are a plasma current of 340 kA and a toroidal magnetic field of 2.25 T. The plasma edge was defined at a minor radius of 46 cm by the toroidal belt limiter ALT II, which consists of eight movable blades, and covers almost the whole inner circumference of the torus, being located at a poloidal angle of -53° below the equatorial midplane. The main poloidal limiters were withdrawn during all shots.

Figure 7 shows a radial ion temperature profile of C^{6+} for a 'standard Ohmic' discharge with a long flat-top phase of more than two seconds. The charge exchange line profiles were integrated over the entire stationary plateau. The line averaged central electron

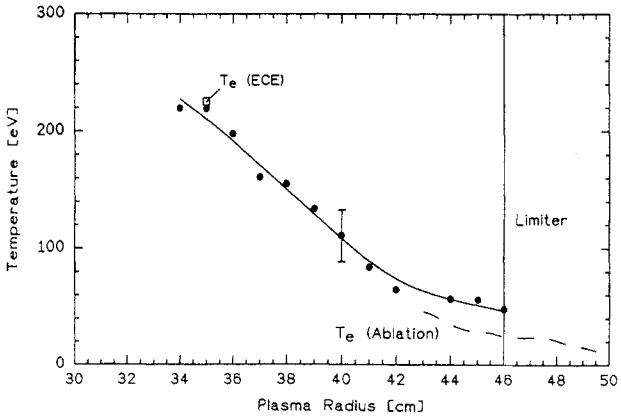

FIG. 7. Radial ion temperature profile of C^{6+} during the flat-top phase of an ohmically heated TEXTOR D_2 discharge compared with the electron temperature. The line averaged central electron density was 3×10^{13} cm^{-3}.

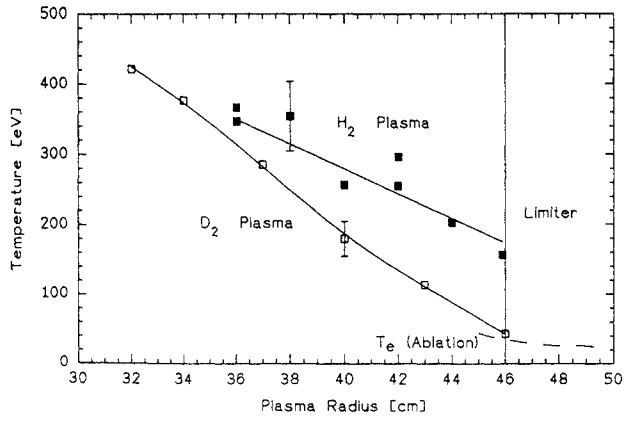

FIG. 8. Radial ion temperature profiles of C^{6+} during hydrogen beam injection of 1.7 MW into H_2 and D_2 plasmas with a line averaged central electron density of 2.5 × 10^{13} cm^{-3}. For comparison, the electron temperature as measured by laser ablation of multilayer targets in the scrape-off layer for D_2 discharges is shown.

density was 3 × 10^{13} cm^{-3}. Also plotted, for comparison, is the electron temperature obtained from electron cyclotron emission [15] and by means of another atomic beam method — laser ablation of multilayer targets [16]. Well inside the limiter position, at r = 35 cm, the electron temperature matches the C^{6+} temperature quite well; however, near the limiters, at r > 42 cm, kT_{C6+} exceeds kT_e by roughly 50–100%.

TEXTOR plasmas with additional heating by injection of hydrogenic neutral beams have also been studied. We have used co-injection at a power of 1.7 MW into deuterium and hydrogen plasmas with a line averaged central electron density of 2.5 × 10^{13} cm^{-3}. Using different discharge gases (D_2 and H_2), we have studied the appearance of the 'isotopic effect' [17], also with regard to impurity ion temperatures. Figure 8 shows kT_{C6+} profiles for the neutral injection phase of these shots. Near the limiters, the two kinds of plasma show almost no difference in temperature between the additional heating phase and the Ohmic pre-phase; the temperature profile for the latter phase is very similar to that for pure Ohmic heating shown in Fig. 7 for D_2 and is therefore not contained in Fig. 8. Inside a minor radius of 42 cm, however, the carbon temperatures rise during neutral beam injection (NBI) heating by more than a factor of two with respect to Ohmic heating. The fact that the edge temperatures remain low during NBI can be explained by an elevated electron density in this phase and an increased carbon concentration, both leading to enhanced cooling of the plasma boundary. In all heating phases studied, the C^{6+} edge temperatures measured in the hydrogen discharges are elevated by a factor of up to four compared to the deuterium shots. Inside r = 38 cm, however, no major difference between H_2 and D_2 can be seen. A similar isotopic dependence has been found previously for electron temperatures in Ohmic TEXTOR discharges [18]. The impurity ion temperatures roughly match the electron temperatures during NBI heating, at least for deuterium plasmas directly in the boundary (see Fig. 8).

7. CONCLUSIONS AND SUMMARY

Some interesting conclusions can be drawn from these proof of principle measurements.

(1) We can compare the C^{6+} temperatures obtained by means of Li-CXS with other plasma temperatures. The equipartition time t_{eq}, i.e. the time necessary to equilibrate the Maxwellian temperatures of two different particle species "f" and "z" by collisions, is derived from Spitzer [19]:

$$t_{eq}\,[s] = \frac{7.34 \times 10^6\, A_f A_2}{N_f Z_f^2 Z_2^2 \ln\Lambda} \left(\frac{kT_f}{A_f} + \frac{kT_2}{A_2}\right)^{3/2} \qquad (9)$$

with

$$\Lambda = \frac{1.55 \times 10^{10}}{Z_f Z_2} \sqrt{\frac{(kT_e)^3}{N_e}} \qquad (10)$$

$A_{f,2}$ denote the atomic masses (in amu) and $Z_{f,2}$ denote the nuclear charges of the respective particles, N_e is the electron density and N_f is the density (in cm^{-3}) of the dominating species f ('field particles', here $N_{C6+} \ll N_f = N_e \approx N_{D+}$), $kT_{e,f,2}$ are the temperatures of the different species (in eV). Assuming typical N_e and T_e profiles for the TEXTOR boundary, i.e. 1 × 10^{12} to 3 × 10^{13} cm^{-3} and 30–500 eV, and taking $kT_f = kT_2 = kT_e$, we calculate from Eqs (9) and (10) an equilibration time of 27–53 μs for C^{6+}/D^+ collisions, while we obtain 1.3–2.5 ms for collisions between C^{6+} and the plasma electrons, using A_f = 1/1823. To reach thermal equilibrium, the collision partners under consideration must remain in the plasma boundary for at least t_{eq}, i.e. the time of equipartition has to be small with respect to the edge confinement times, which have been determined to be of the order of 1 ms in TEXTOR. Accordingly, the C^{6+} ions have sufficient time during their stay in the plasma edge to reach a temperature equilibrium with the plasma deuterons. Thus, Li-CXS

is an excellent tool for determining the ion temperature of a fusion edge plasma with reasonable spatial and perhaps temporal resolution because, instead of D^+, we can analyse an impurity species, which is more easily accessible by means of optical methods. However, C^{6+} particles need considerably more time to reach equilibrium with the plasma electrons. In this case, t_{eq} may exceed the edge confinement time by more than a factor of two. Consequently, kT_{C6+} is not expected to be equal to the electron temperature under all circumstances, as can be seen, for example, in Fig. 7, especially at minor radii >40 cm.

(2) We can estimate the amount of physical $C^{6+} \rightarrow C$ self-sputtering that contributes to the erosion of limiter surfaces by applying a simple model. C^{6+} ions will be accelerated towards neutral solid structures by a plasma sheath potential of $6 \times 3kT_e$. In the Ohmic case (see Fig.7) we have $kT_e = 25$ eV at a limiter position of $r = 46$ cm, leading to a potential of 450 eV. Hence, the stripped carbon nuclei hit the ALT II limiter blades with mean energies [20] of $\langle E \rangle = 6 \times 3kT_e + 2kT_{C6+} = 550$ eV, using $kT_{C6+} = 50$ eV as measured at the limiter radius. The flux density $\Phi_{C6+\rightarrow C}$ of sputtered neutral carbon due to C^{6+} bombardment can be expressed according to Ref. [21] as

$$\Phi_{C6+\rightarrow C} = Y(\langle E \rangle)\, N_{C6+} C_S \cos\vartheta \qquad (11)$$

with

$$C_S = \sqrt{\frac{kT_{C6+} + kT_e}{m_{C6+}}} \qquad (12)$$

being the ion acoustic velocity at the plasma sheath. N_{C6+} denotes the absolute density of C^{6+}, and $Y(\langle E \rangle)$ is the carbon self-sputtering yield. ϑ is the mean angle between the ALT II limiter surface and the magnetic field lines, corresponding to the orientation of ion bombardment. The value of ϑ has been determined by means of numerical modelling [22] to be 88.9°, averaged over the surface of a single ALT II blade. Using the C^{6+} densities published in Ref. [2] for the same type of Ohmic shots as studied in Fig. 7 (2.4×10^{10} cm^{-3} at the limiter radius), as well as the self-sputtering yields published in Ref. [23] for normal incidence ($Y = 0.30$ at an ion energy of 550 eV, neglecting geometric surface structures) and an ion acoustic velocity of 2.5×10^6 cm·s^{-1}, taken from Eq. (12), we derive a flux density of sputtered carbon of 3.7×10^{14} cm^{-2}·s^{-1}, which is exclusively caused by C^{6+} irradiation.

The total fluxes of neutral carbon released from the ALT II surface have been measured in parallel by means of optical emission spectroscopy [24, 25], delivering an absolute value of 3×10^{15} cm^{-2}·s^{-1}. Therefore, fully stripped carbon nuclei are estimated to contribute to the erosion of the ALT II surface up to 12% during the Ohmic shots studied. A more sophisticated investigation, taking into account also bombardment by lower ionization states of carbon and carbon release by deuterium irradiation, seems feasible, employing Li-CXS also for other types of discharges; this is, however, outside the scope of the present paper.

Li-CXS is especially suited to investigate edge plasmas of present day tokamaks, which have electron densities between 1×10^{12} and 3×10^{13} cm^{-3}. In these tokamaks, beam penetration depths of more than 20 cm can easily be achieved with acceleration voltages below 30 kV, which can still be handled safely from the engineering point of view. Considering, however, a hypothetical application of Li-CXS to NET/ITER, the beam energy has to be increased to approximately 300 keV in order to maintain a length of 20 cm (assuming a central N_e of 5×10^{14} cm^{-3}, a central T_e of more than 8 keV, a minor radius of 2.15 m and parabolic profile shapes). In spite of these problems the development of an appropriate lithium beam source delivering a current density of at least 10 mA/cm^2 would be a technical challenge, because the basic understanding of impurity transport in boundary plasmas, being a major topic of today's tokamaks, could perhaps be improved with this kind of diagnostic method applied to a future machine.

In summary, we have demonstrated the potential of Li-CXS to measure temperatures of C^{6+} impurity ions in the outermost 15 to 20 cm of ohmically heated and beam heated TEXTOR discharges. We have shown that the values obtained can be considered to be equal to those of deuterium or hydrogen ions. A first attempt to quantitatively analyse the $C^{6+} \rightarrow C$ self-sputtering on limiter surfaces shows that a fraction of roughly 12% of the total carbon erosion originates from this specific process during the stationary flat-top phase of medium density Ohmic shots. Thus, besides delivering absolute density profiles of highly charged impurity ions, which is of relevance in verifying the theoretical modelling of edge transport [26], Li-CXS seems to be capable of contributing also to the study of impurity release.

ACKNOWLEDGEMENT

Participation of the group from the Technische Universität Wien has been supported by the Kommission zur Koordination der Kernfusionsforschung at the Austrian Academy of Sciences.

REFERENCES

[1] WINTER, H., Comments At. Mol. Phys. **12** (1982) 165.
[2] SCHORN, R.P., HINTZ, E., RUSBÜLDT, D., AUMAYR, F., SCHNEIDER, M., UNTERREITER, E., WINTER, H., Appl. Phys. B **52** (1991) 71.
[3] WOLFRUM, E., HOEKSTRA, R., HEER, F.J. de, MORGENSTERN, R., WINTER, H., Absolute visible light emission cross-sections for electron capture from Li atoms by slow, highly charged ions, to be published in J. Phys. B.
[4] JANEV, R.K., Phys. Scr., T **3** (1983) 208.
[5] JANEV, R.K., BRANSDEN, B.H., GALLAGHER, J.W., J. Phys. Chem. Ref. Data **12** (1983) 829.
[6] BÖTTICHER, W., in Plasma Diagnostics, North-Holland, Amsterdam (1968) 650.
[7] MOORE, C.E., Atomic Energy Levels I, NBS Circular 467, National Bureau of Standards, Washington, DC (1949).
[8] SOMMERFELD, A., Atombau und Spektrallinien, Vol. 1, Vieweg, Braunschweig (1960) 578.
[9] FONCK, R.J., DARROW, D.S., JAEHNIG, K.P., Phys. Rev., A **29** (1984) 3288.
[10] BASHKIN, S., STONER, J.O., Jr., Atomic Energy Levels and Grotrian Diagrams, Vol. 1, North-Holland, Amsterdam (1975) 96.
[11] BURGESS, A., SUMMERS, H.P., Mon. Not. R.A.S. **226** (1987) 257.
[12] SUMMERS, H.P., Atomic Data and Analysis Structure Software Package at JET, Version 1.0 (1990).
[13] BETHE, H.A., SALPETER, E.E., in Handbuch der Physik, Vol. 35, Atome I, Springer-Verlag, Berlin (1957) 359.
[14] BAY, H.L., DULLNI, E., LEISMANN, P., Characteristics of a High Current Ion Source Operated with Lithium, Rep. Jül-2062, Kernforschungsanlage Jülich (1986).
[15] WAIDMANN, G., CAO, Y., KARDON, B., Plasma Phys. Control. Fusion **31** (1989) 323.
[16] POSPIESZCZYK, A., ROSS, G.G., Rev. Sci. Instrum. **59** (1988) 605.
[17] BESSENRODT-WEBERPALS, M., McCORMICK, K., WAGNER, F., ASDEX Team, J. Nucl. Mater. **176&177** (1990) 538.
[18] SAMM, U., BOGEN, P., HARTWIG, H., et al., in Controlled Fusion and Plasma Physics (Proc. 16th Eur. Conf. Venice, 1989), Vol. 13B, Part III, European Physical Society (1989) 995.
[19] SPITZER, L., Jr., in Physics of Fully Ionized Gases, 2nd edn, Interscience Publishers, New York (1967) 135.
[20] MATTHEWS, G.F., J. Nucl. Mater **162-164** (1989) 38.
[21] STANGEBY, P.C., in Physics of Plasma-Wall Interactions in Controlled Fusion, Proc. NATO Advanced Study Institute Val-Morin, Quebec, 1984), NATO ASI Series, Vol. 131, Plenum Press, New York (1986) 41.
[22] BAEK, W.Y. (KFA, Jülich) personal communication, 1991.
[23] ROTH, J., BOHDANSKY, J., OTTENBERGER, W., J. Nucl. Mater. **165** (1989) 193.
[24] POSPIESZCZYK, A., PHILIPPS, V., KÖNEN, L., SAMM, U., J. Nucl. Mater. **176&177** (1990) 180.
[25] BOGEN, P., HARTWIG, H., HINTZ, E., et al., J. Nucl. Mater. **128&129** (1984) 157.
[26] CLAASSEN, H.A., SCHORN, R.P., GERHAUSER, H., J. Nucl. Mater. **176&177** (1990) 398.

(Manuscript received 20 August 1991
Final manuscript received 19 November 1991)